Hindawi
International Journal of Energy Research
Volume 2024, Article ID 3395861, 19 pages
https://doi.org/10.1155/2024/3395861

Research Article

Combustion Characteristic Prediction of Dual Direct Injection Fuel (Diesel-Propane) on RCEM Based on an Artificial Neural Network Approach

Ardhika Setiawan[1] **and Ocktaeck Lim**[2]

[1]*Graduate School of Mechanical Engineering, University of Ulsan, San 29, Mugeo-dong, Nam-gu, Ulsan 44610, Republic of Korea*
[2]*School of Mechanical Engineering, University of Ulsan, San 29, Mugeo-dong, Nam-gu, Ulsan 44610, Republic of Korea*

Correspondence should be addressed to Ocktaeck Lim; otlim@ulsan.ac.kr

Received 18 October 2023; Revised 4 January 2024; Accepted 7 March 2024; Published 12 April 2024

Academic Editor: Hock Jin Quah

Studies from around the world show that engines using biofuel, LPG, and CNG emit fewer pollutants than those using conventional fuels. Experimental research has focused on a rapid compression and expansion machine (RCEM) that resembles a compression ignition (CI) engine. It uses dual direct injection fuel, diesel and propane (DP), with propane injection timing varying from 0 to 40 before top dead center (BTDC) and diesel injection timing remaining at 10 BTDC. The compression ratio was changed at points 17 and 19 by adjusting the RCEM connecting rod. A converge simulation program was used to run the simulation model, which was used to examine how the fire and inflow inside the chamber developed. The ANN method was used to predict pressure, temperature, power, TKE, and ITE data output based on propane energy fraction, compression ratio, and SOI of propane as input data parameters. It was noticed that the ANN prediction on experimental data has a higher accuracy compared to the simulation prediction. The R and MSE values were used to identify the accuracy of the prediction on output parameter data. ANN generalization capability is comparatively high when trained with large enough databases. The highest accuracy of prediction was produced on TKE, which had an MSE of 0.003715 and R value of 0.99981 from 287900 sample data. This shows that the ANN model is quite accurate in forecasting output experimental data.

1. Introduction

Researchers are focusing on finding substitutes for traditional petroleum fuels due to environmental concerns and the depletion of petroleum resources. Reserves are depleted, and air pollution rises as a result of excessive use of fossil fuels. These problems prompt the need for efficient use of current resources and gradual transition to environmentally friendly alternative fuels [1, 2]. Utilizing gaseous fuels in a compression ignition (CI) engine in addition to liquid diesel is one way to achieve this. CI engines heat the air in the engine cylinder more efficiently than a dual spark injection (SI) engine because of its higher compression ratio. The fuel is then introduced and spontaneously ignites. The fuel is typically diesel, which is denser than propane. Diesel engines outperform propane engines for two reasons: (i) higher cylinder pressures and correspondingly higher temperatures improve the thermal efficiency of the diesel engine and (ii) diesel engines do not use the air throttling required to regulate the propane engine's power output because it lowers engine efficiency [3]. This makes the CI engine more popular in industry and as a study topic for the researchers.

LPG is a readily available, portable, clean, and efficient energy source for consumers all over the world. Although it is increasingly produced from renewable sources, LPG is primarily obtained from natural gas and oil production. Studies from around the world show that engines using biofuel, LPG, and CNG emit fewer pollutants than those using conventional fuels [4, 5]. When the ambient temperature is normal, LPG is liquid at about 8 bar. Propane vapor pressure is about 20 bar at 55°C, which is still a moderate pressure at the higher end of typical ambient temperatures, making

storage feasible [6, 7]. Moreover, LPG contains higher calorific value compared to diesel fuel, which makes it have a higher volumetric efficiency when stored into the storage tank. LPG is made of a variable mixture of propane (C_3H_8), propylene, and butane (C_4H_{10}), whose ratios are changed throughout the year to produce the best combustion properties at various ambient temperatures [8]. Propane is unaffected by cold winter temperatures because it has a higher calorific value than butane and a much lower boiling point. For that reason, the usage of 100% propane is preferable in vehicles to maintain the stability of the phase of the fuel and better energy conversion.

The dual-fuel combustion strategy, as its name implies, uses two different fuels, typically diesel and natural gas, and is one of the most recent technologies to be developed. Compared to conventional diesel engines or dual direct injection-ignited engines, dual-fuel engines offer a variety of benefits [9, 10]. Diesel fuel's ability to self-ignite and natural gas' low rate of pollution are combined to create an intriguing power to pollution ratio. Numerous studies on the creation, fabrication, and modelling of dual-fuel engines have been published [10–12]. Different engine manufacturers have incorporated dual-fuel technology into a variety of products (cars, power plants) as a whole or as an added feature.

Due to a driving system that was electrically controlled and hydraulically actuated, the rapid compression-expansion machine (RCEM) was able to mimic a comparable combustion process in a single diesel cycle [13]. The ability to compress and expand in RCEMs results in closer in-cylinder pressure characteristics with the real engine compared to a rapid compression machine (RCM) and shock tube. RCEM has the stability to be modified to fit the condition of an experiment, such as compression ratio, combustion strategy (CI, SI, SPCCI, and dual injection), temperature control, and ambient gas condition setting, making it a preferable experimental engine for researchers to explore wide range of topics.

LPG has been suggested as a potentially effective substitute for diesel engines in reducing particle emissions and eventually NOX emissions [14]. However, its low cetane number causes problems [15]. The possibility of increasing the LPG cetane number (CN) through the addition of cetane number improvers was investigated by researchers [16]. According to Hashimoto et al., there are two ways to increase the CN of LPG: either by adding 1% m/m cetane number improvers or by combining LPG with 30% m/m n-paraffins and 15% m/m cetane improvers [17]. On the other hand, some writers recommended converting from diesel to LPG fuel by using diesel dual-fuel (DDF) systems [18, 19]. Because LPG has a very low cetane number, it requires a pilot diesel injection to make sure the blend ignites and the LPG burns afterwards.

LPG has a very low temperature when stored into an LPG tank. Thus, it should be maintained in a liquid phase to maximize the quantity of the fuel in storage. The intake manifold injection strategy of LPG will reduce the intake temperature significantly. This minimizes the volumetric efficiency and degrades the autoignition characteristics of the diesel. The intake manifold system is unable to achieve high LPG substitution ratios due to the knock ability of mixtures with high percentages of LPG [20]. It is important to find an efficient position of injection timing based on the characteristics of the fuel. Early direct injection produces an extended ignition delay that provides a better air-fuel mixture before autoignition occurs. However, in the case of liquid phase of LPG, early injection will reduce the temperature significantly and disturb the ignition of the diesel. For that reason, it is important to investigate suitable injection timings for direct injection of LPG.

Researchers have turned to techniques that can achieve the same performance more quickly and inexpensively because traditional methods are time-consuming and costly [21]. ANN has been applied for a variety of automotive engineering issues in the modern era as a result of advancements in computer technology. Numerous studies utilizing only ANN in diesel engines can be found in the literature. A system that mimics how nerve conduction works in the human brain is known as an ANN [22, 23]. Information flow in the context of ANN is provided by three layers. Grosan et al. and Srinidhi et al. [22, 24] used dual fuel to compare the performance parameter results of the internal combustion engine with ANN data. They developed an ANN model with high accuracy values, demonstrating its applicability for the prediction of experimental data. Srinidhi et al. [23] created an ANN model for the spark timing of an internal combustion engine. They discovered that the ANN model performed well in controlling spark timing. Additionally, an increase in the engine's thermal and combustion efficiencies was noted. Srinidhi et al. [24] compared experimental emission and performance findings with findings from ANN model predictions. High accuracy values in this study were obtained as a result of the comparison.

Some researchers have studied LPG-diesel used in dual-fuel engines with CI engines [20, 25, 26]. The majority of the studies were restricted to LPG intake manifold injection strategy, with a small range of energy fraction variation and timing of LPG injection. There is thus an opportunity to identify a more effective plan of action to raise the standard of diesel-LPG fuel combustion. This experimental investigation was conducted in a single-cylinder RCEM fueled with dual direct injection fuel (propane and diesel). The focus of this work was on determining the operating range for the energy substitution ratio and compression ratio. Variations in the timing of propane injection and the combustion properties of each range bound were also examined. Furthermore, the effect of propane direct injection strategy on the in-flow phenomenon was analyzed using CFD simulation.

2. Methodology

2.1. Engine Setup. The rapid compression-expansion machine (RCEM) is a highly developed device that replicated a similar combustion mechanism in a diesel cycle using a hydraulically and electrically controlled driving system [13]. A single cycle, rapid compression stage of a test fuel can be analyzed in an RCM/RCEM under precisely

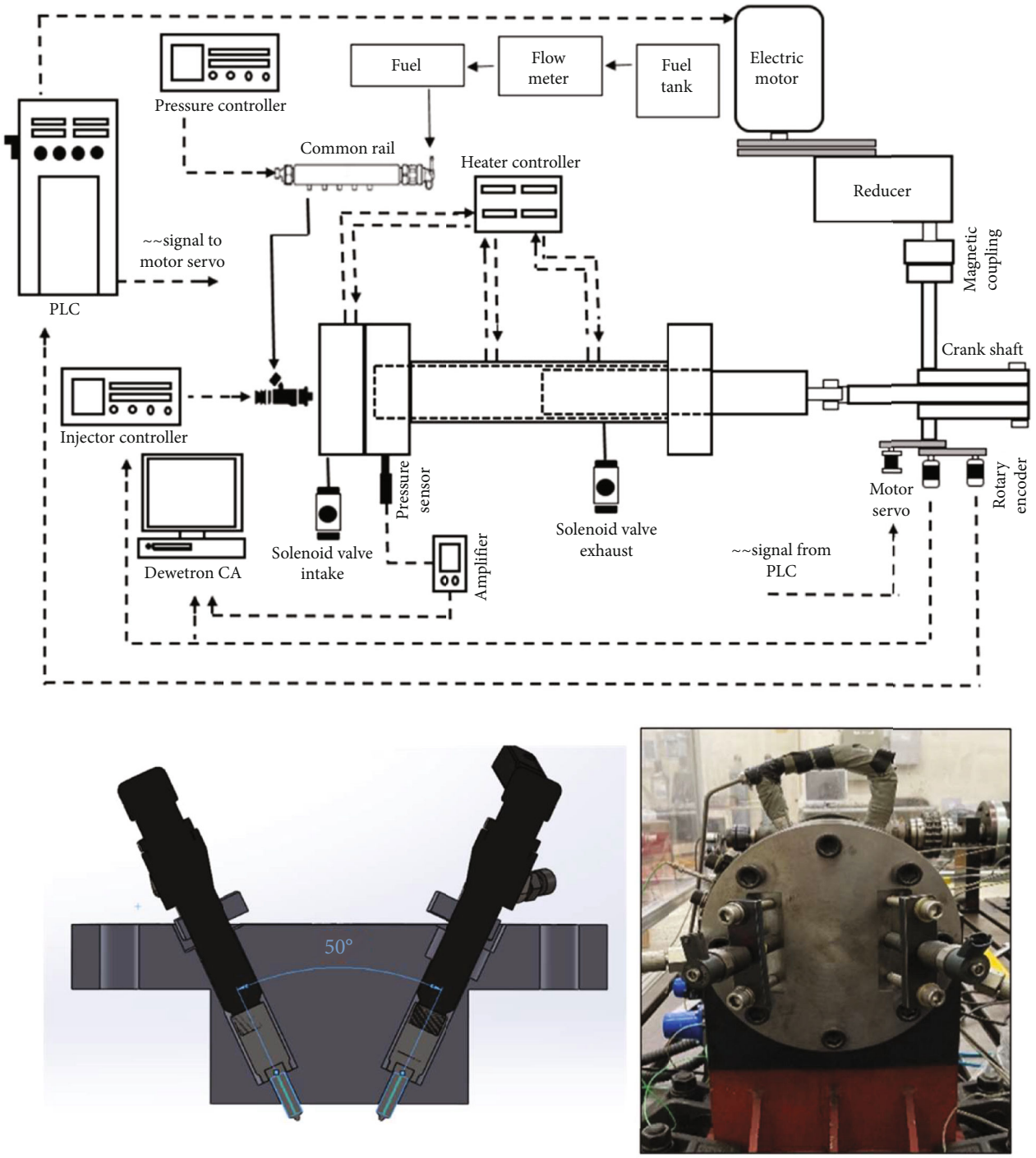

Figure 1: Schematic diagram of RCEM.

defined and controlled conditions without complicated fluid dynamics characteristics of an internal combustion engine [27]. The ignition strategy can be modified by changing the cylinder head to satisfy the requirement of compression ignition or dual direct injection ignition engine. In the current study, the cylinder head was modified to fit two direct injection strategies using diesel and LPG as the fuel. The RCEM schematic is shown in Figure 1. With a 100 mm bore and 450 mm stroke, it has a single-cylinder engine coupled to a 22 kW electric motor. The electric motor is able to run 1200 rpm at full power. The motor is coupled to the gearbox to reduce the rotation of RCEM to 240 rpm coupled with a magnetic clutch to transfer sudden energy to the crankshaft. The crankshaft base contains a screw that can be turned to alter the compression ratio, which is adjustable from 10 to 27.

Temperature sensors and controls were attached in the body, TDC, and BDC to maintain the temperature's consistency, which could reach a maximum of 393 K. A Kistler 5018 amplifier and a Kistler 6052CU20 pressure transducer were used to monitor the engine's pressure. Table 1 displays engine specifications. The in-cylinder pressure was measured using an amplifier of Kistler type 5018 and a piezoelectric pressure transducer of Kistler type 6052CU20 with a reading accuracy of 0.005. To measure the crank angle position, an Autonics rotary encoder with a 0.1 degree resolution of crank angle was installed. The sensors were attached to a Dewetron type DEWE800-CA acquisition device in order to obtain the data.

2.2. Test Procedure. The RCEM was used for the experiments, and the cylinder head was modified to allow for the installation of dual injectors. Three heater bands were installed in the cylinder body, and one heater band was attached to the cylinder head. The in-cylinder temperature was maintained at 353.15 K, which implies that this is the warm-up end point from the aspect of engine stabilization [28]. This temperature was maintained for at least 30 minutes to ensure the homogeneity distribution of heat in the cylinder. The compression ratio can be controlled by adjusting the screw of the connecting road to compare the moving stroke and in-cylinder volume. The compression ratios used in this study were 17 and 19. To maximize the sudden force of the RCEM mechanism, the rod shaft was connected to the 22 kW electric motor at a maximum speed of 1200 rpm. This speed was then reduced by the gearbox to 240 rpm. The piston was set to bottom dead center (BTDC) at the beginning of the experiment. A magnetic clutch delivered the force from the electric motor to the connecting road for 360° of rotation, and the in-cylinder pressure was recorded.

The main fuel used in this investigation was an LPG consisting of 99.99% propane and conventional diesel that were obtained from a local fuel station in Korea. Information related to fuel physical properties is provided in Table 2 [29]. The fuels are identified as "DP10 to P100" representing propane and diesel energy composition. Here, "P" represents propane, "D" represents diesel, and the number in the last digit represents the percentage of propane energy. The injection rate test was performed on the fuel injection rate device depicted in Figure 2 to verify the volume of fuel injected into the chamber. A Bosch 7-hole injector 0445110 327 and a Denso 0221 were connected to the fuel injection rate device, and the rate of injection flow was calculated. A Zenobalti multistage injection controller ZB-8035 in conjunction with a common rail solenoid injector peak and hold driver of type ZB-5100 were used to internally activate the injector solenoid to control the SOI timing. A PCV driver ZB-1100 for a common rail and an electric motor controller both kept the injection pressures at 30 bar by controlling them with common rail controllers and high-pressure injection pumps, respectively. 500 cycles of injection rate test were performed beforehand to obtain the same amount of energy from fuel with 0.5 of an equivalence ratio. Table 2 shows the physical properties of the fuel.

Table 1: Engine specifications.

Bore × stroke	100 × 450 mm
Connecting road	900 mm
Compression ratio	10 : 1–27 : 1
Number of nozzle holes	7
Injector diesel	A Bosch 0445110327
Injector propane	Denso 0221
Motor speed	1200 rpm
Crank shaft speed	240 rpm
Temperature control	323.15–413.15 K
Fuel injection system	Common rail direct injection (CRDI)

Table 2: Fuel physical properties.

Properties	Propane	Diesel
Molecule formula	C_3H_8	$C_nH_{1.8n}$
Boiling point (°C)	-42.1	180-370
Stoichiometric A/F	15.71	14.6
Autoignition temperature (°C)	481	250
Lower heating value (MJ/kg)	46.34	42.5
Research octane number	111	—
Cetane number	—	40-55

There are two stages of pressurization required before direct injection of LPG fuel can begin: the first is carried out using a fuel tank-mounted electric low-pressure pump and the second is carried out using a high-pressure plunger pump. The fuel pressure is raised to 8 bar in the first stage and 200 bar in the second stage. It is necessary to maintain the LPG in its liquid phase in order for the fuel pump to work properly. In this regard, the current study determined that the fuel injection pressure should be 200 bar, taking the durability and performance of the pump into consideration. Meanwhile, the injection pressure for the diesel was maintained at 500 bar. The diesel fuel is considered as the ignitor of the combustion and maintained the injection timing at 10° BTDC. To find the best combustion characteristics produced by the LPG, the injection timing varied from early injection (40° BTDC) to late injection (0° BTDC). To determine the most efficient fuel composition, a wide range propane percentage from 10% up to 100% was applied based on the low heating value comparison with the diesel. The details of the current study can be seen in Table 3.

2.3. CFD Modelling and Simulation. CONVERGE CFD software was used in this study to simulate internal combustion engine processes. Advanced numerical methods and physical models of the spray, turbulence, and combustion processes, as well as their nonlinear interactions, are included in CONVERGE. To better understand the behavior of combustion in dual-fuel engines, dual-fuel combustion was modelled. Surfaces for the geometry were produced both before and after simulation using a full mesh construction method. Using the methods of fixed embedding, adaptive mesh

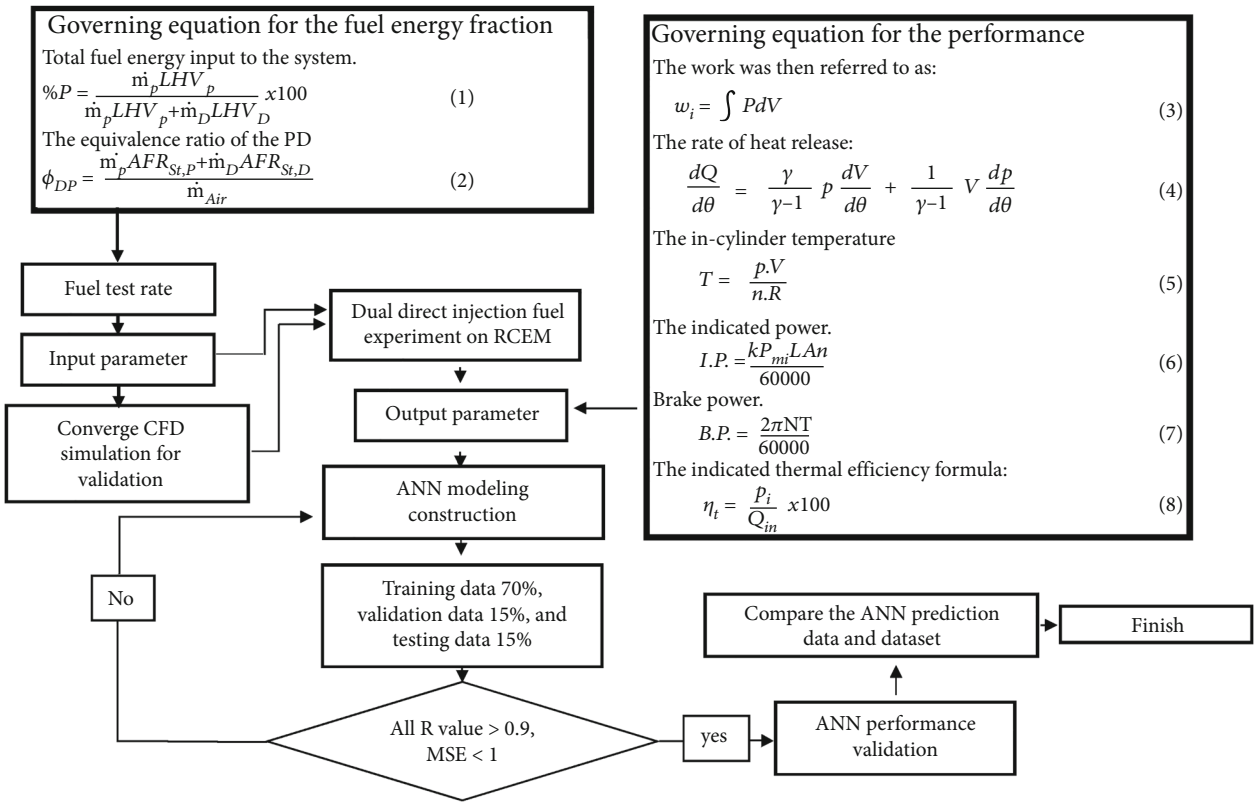

Figure 2: Flow chart of the study.

Table 3: Experimental conditions.

Properties	Diesel	Propane
Injection pressure (bar)	500	200
Fuel injection timing (BTDC)	10°	0°–40°
Fuel percentage	0-90%	10-100%
Initial pressure	1 atm	
Compression ratio	17 and 19	
Initial temperature (K)	353.15	
Engine speed (rpm)	240	

refinement subdivision (AMR), and basic grid size, we modified the grid size and the total number of grid cells.

CONVERGE CFD 3.0 was used for the computational analyses. Closed cycle simulations were carried out using the combustion chamber's full sector geometry. A turbulence model must be used to obtain accurate CFD simulation results because turbulence has a significant impact on the rate at which momentum, energy, and species mix. The renormalization group (RNG) k-ε turbulence model [30] performs better than the standard k-turbulence model for describing anisotropic and nonequilibrium effects. To use the discretized Navier-Stokes equation on the Cartesian grid, a finite volume indirect discretization method was selected. Table 4 shows the detail parameters input for the current CFD modelling. To save time, the computer simulates all three processes: combustion, compression, and expansion. Utilizing information gleaned from experimental observations, the initial fuel, ambient temperature, and air conditions were specified. The initial fields of temperature, flow velocity, and pressure were generated until the motoring pressure from the experiments was met. Figure 3 shows the schematic diagram of RCEM in-cylinder chamber on CFD modelling.

2.4. ANN Construction. An ANN-based model for the factors affecting combustion has been developed. The experimental study's degree of error was determined using the ANN model. For the combustion parameters, the findings of an ANN were compared with those of an experimental investigation that used FEBRIS analysis.

A computing system called an artificial neural network (ANN) was constructed to stimulate and process data in a manner similar to how the human brain does it. It employs artificial intelligence (AI) to find solutions to issues that are intractable or challenging for people [36]. Neurons are closely interconnected in a number of layers in an ANN system with the number of layers depending on the difficulty of the problems. Each neuron has a weight and bias that are assigned to it. Multilayer perceptron (MLP), also known as multilayer neural networks, is the most well-known example of this type of neural network. The layers between the input and output layers are referred to as hidden layers, and they have a significant impact on how well the developed ANN predicts outcomes. An artificial neural network (ANN) system is a device that receives input, processes the data, and outputs the results. The input is comprised of an array of

Table 4: CFD parameter input.

Phenomenon	Model
Turbulence flow	RNG k-ε [30]
Drop drag	Dynamic drop drag [31]
Break-up	KH-RT [32]
Drop collision	NTC [33]
Drop evaporation	Frossling [34]
Drop turbulent dispersion	TKE preserving [31]
Chemistry solver	SAGE [35]

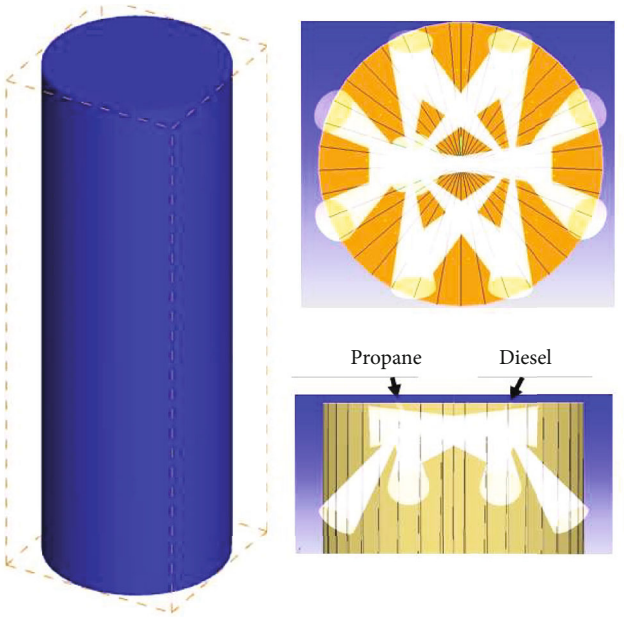

Figure 3: Schematic diagram of RCEM for CFD investigation.

data. When an input is sent to a neural network and a matching desired or target response is set to the output, an error occurs when there is a discrepancy between the desired response and the actual system output. The system uses the error as input and modifies all of its parameters in accordance with a learning rule (backpropagation). Until the intended outcome is achieved satisfactorily, this process is repeated (in iterations or epochs). By utilizing the gradient descent method, the backpropagation algorithm refines the model and increases the degree of agreement between the predicted and actual values. A straightforward model of the process element that was inspired by biological neurons is shown in Figure 4. In this model, i, the output of the process element is given in

$$y(t+1) = a\left(\sum_{j=1}^{m} w_{ij}x_j(t) - \Theta_i\right), \tag{1}$$

where i is the processing element's threshold value and $(.)$ is the activation function. Input and output make up the two components of the processing element information processing. By combining the input data x_j received from the outside over the w_{ij} weights to which they are connected, a processing element produces a net value. The net value of the processing element is calculated using

$$\text{met} = \left(\sum_{j=1}^{m} w_{ij}x_j - \Theta_i\Theta\right). \tag{2}$$

In the current study, MATLAB/artificial neural network module was used to train the feed-forward multilayer ANN model. The input layer, output layer, and hidden layer are the three layers that make up an ANN, which can have any number of layers [24], as shown in Figure 5. All the input parameters are contained in the input layer. The hidden layer computes the data from the input layer, and the output layer computes the output vector that follows. The estimation process using the ANN technique entails three sequential steps: modelling, learning (or training) phase, and testing phase [37]. The engine's chosen input and output factors were used to build an ANN model during the modelling stage. The network was set up to produce a target prediction based on input data during the training phase. Test results were compared with the estimated data regarding the test procedure. Once the test error reached the desired level, the network's training phase was terminated [24].

The models' estimation success was assessed using regression coefficients and mean square error (MSE), which were developed using the ANN model's targets and outputs. The evaluation was conducted using the following equations:

$$R^2 = 1 - \left(\frac{\sum_{i=1}^{n}(t_i - o_i)^2}{\sum_{i=1}^{n}(o_i)^2}\right),$$
$$\text{MSE} = \frac{1}{n}\sum_{i=1}^{n}(y_i - t_i), \tag{3}$$

where "t" is the actual output, "o" is the estimated output value, and "n" is the number of dots in the data set. An ANN model with a low error rate was developed using experimental data as a basis. In this study, propane injection timing, propane energy ratio, and engine compression ratio were selected as input parameters for the input layer, and mean pressure and smoke were chosen as output parameters for the output layer.

In this study, a neural network was employed for estimating the combustion characteristics of RCEM powered by diesel and propane by a dual direct injection strategy. Energy fraction ratio of propane, propane fuel injection timing, and the compression ratio were selected as input factors, while mean pressure, in-cylinder temperature, power, TKE, and indicated thermal efficiency were selected as output factors. The neural network methodology in this study also applied the same data set, which included 20 test trials. In particular, 70% of the data trials were utilized for neural network training, 15% for verification, and 15% for testing. The ANN was created using the following methods: feed-forward backpropagation network type, mean square error (MSE)

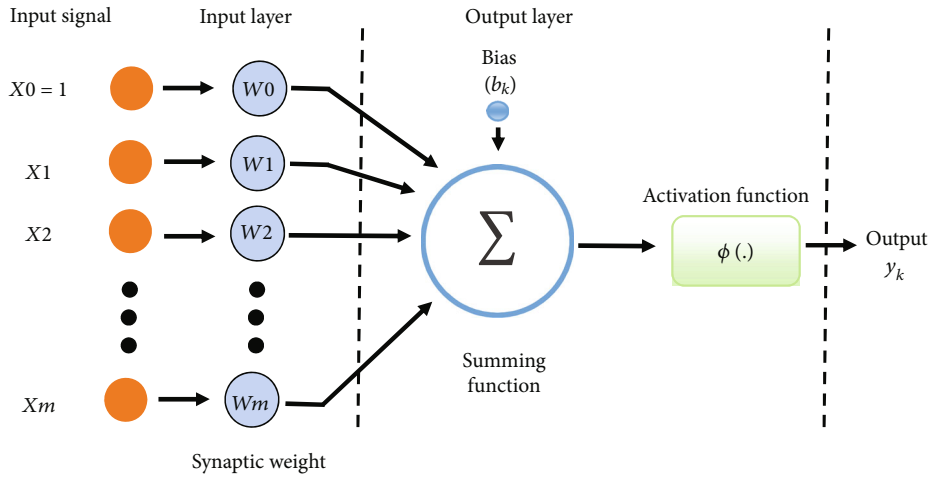

Figure 4: Representation of a model neuron.

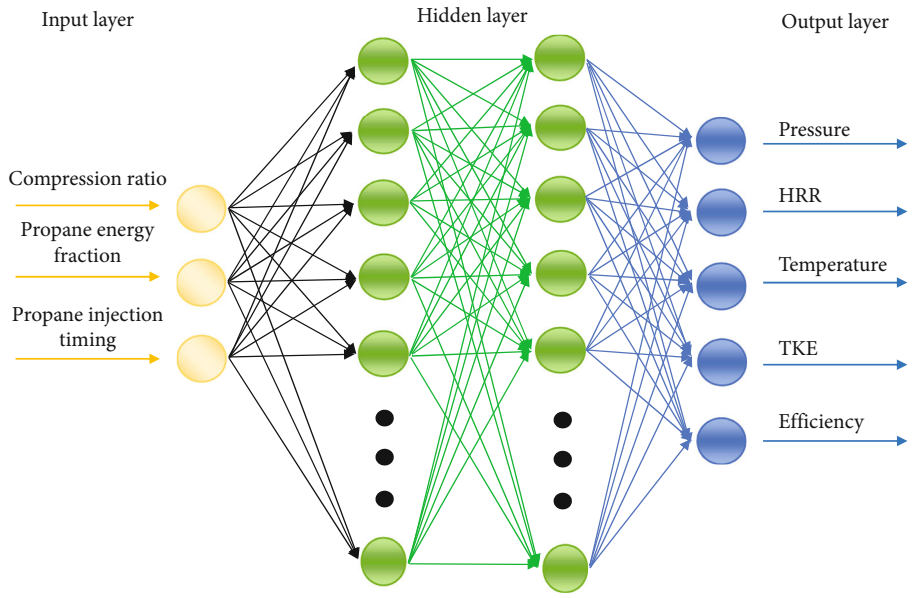

Figure 5: Artificial neural network structure for RCEM.

performance function, logsig transfer function, Levenberg-Marquardt (trainlm) training function, and gradient descent with momentum weight and bias learning function (learngdm). This was done using the feed-forward backpropagation network type, which is typically used to describe challenging system modelling and identification issues. MSE determined the network's failure function using the Levenberg-Marquardt (trainlm) training function, which is typically used for precise estimates [37]. The majority of researchers discovered that the logistic sigmoid activation function (logsig) produces superior results to other functions [38]. Table 5 provides specifics regarding the neural network and the development of the ANN model [39].

3. Results and Discussion

3.1. Input Data Parameter. Figure 6 compares the measured cylinder pressure traces and peak pressures of compression, (a) 17 and (b) 19, and calculated cylinder pressure for five propane injection cases and propane injection quantity cases for 10, 50, and 90% propane energy fractions. Moreover, the measured maximum in-cylinder pressures were compared with their simulated values. The charge's thermodynamic state can be determined from the pressure inside the cylinder using the first law of thermodynamics and a few fundamental presumptions.

We expected to get proper combustion using LPG fuel as it has a low evaporation temperature and higher LHV compared to diesel fuel. Hence, it has better atomization characteristics and produces a higher amount of heat released during combustion. However, in the direct injection strategy, propane was injected to the chamber in liquid phase, which has very low temperature (-43°C). Furthermore, the current common rail system requires much lower fuel injection pressures compared to diesel for safety purposes. Consequently, lower atomization characteristics were produced

Table 5: Particulars of the neural network [39].

Network	3 inputs, 5 outputs, and one hidden layer
Data	Training: 75% randomly selected data from experimental data Test: 25% randomly selected data from experimental data
Network type	Feed-forward backpropagation
Training function	trainlm
Adaptation learning function	learngdm
Transfer function	logsig
Performance function	Mean square error
Stopping criteria	Break the training of network when the confirmation error begins increasing

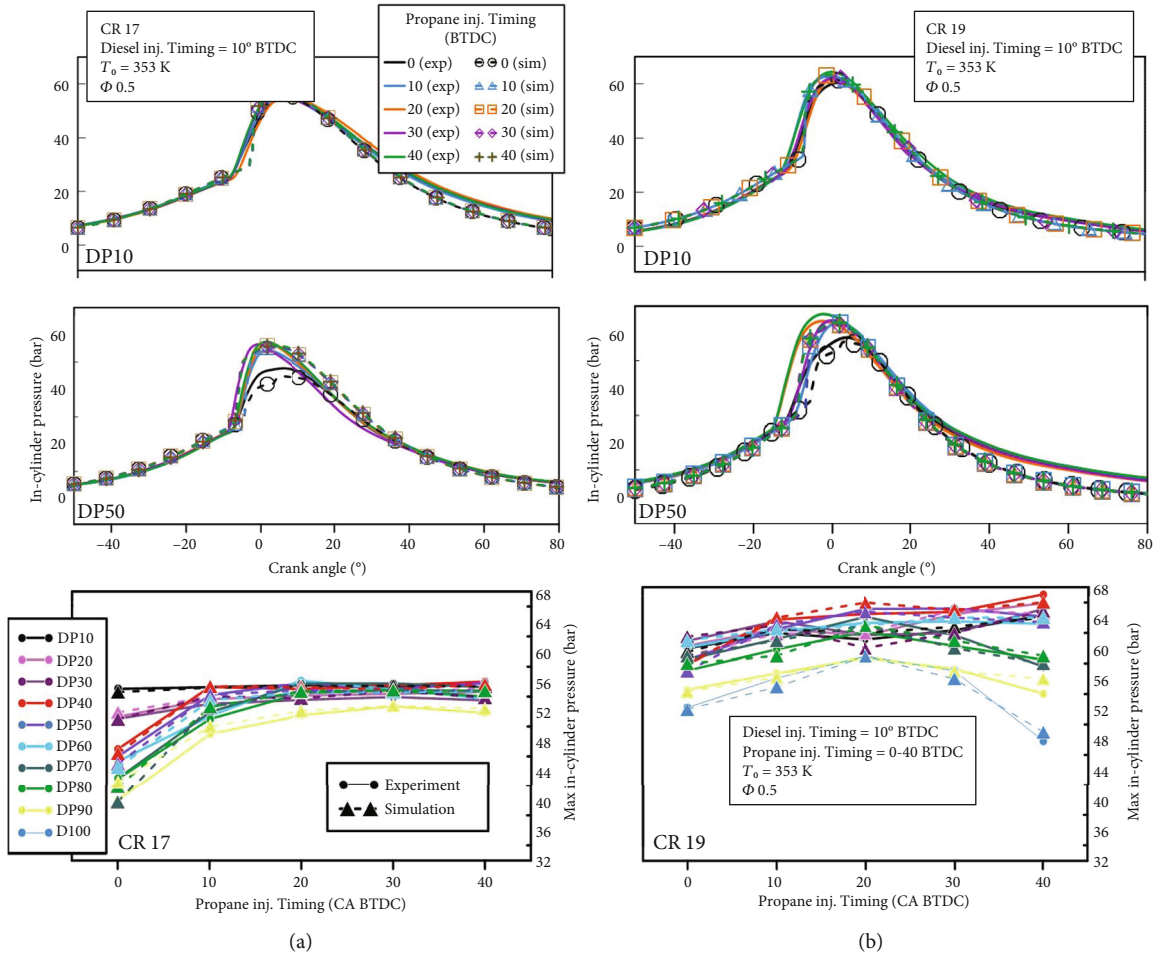

Figure 6: In-cylinder pressure under propane energy fraction 10-100%, propane injection timing 0°-40° BTDC, and compression ratio of (a) 17 and (b) 19.

for propane injection case. It will lower the reactivity of the fuel based on low compression ratio and high quantity of propane. As a result, it will improve the possibility of wall impingement, which reduces cylinder wall temperature. Decreasing the in-cylinder temperature reduced peak cylinder pressure and increasing ignition delay, which agree with those in previous research by Varde [40]. Furthermore, it affects the ambient temperature of diesel injection condition. Low ambient temperature would alter the Sauter mean diameter (SMD) distribution and spray tip penetration, decelerate diesel fuel evaporation, and reduce diesel fuel activation [41].

Figure 7 shows experiment and simulation data in-cylinder temperature under propane energy fraction 10-100%, propane injection timing 0°-40° BTDC, and compression ratios of (a) 17 and (b) 19. Earlier propane injection into the chamber results in lower ambient temperature produced, and it will affect the temperature required for the autoignition event. At the condition of CR17, in the in-cylinder temperature trace, the highest peak temperature

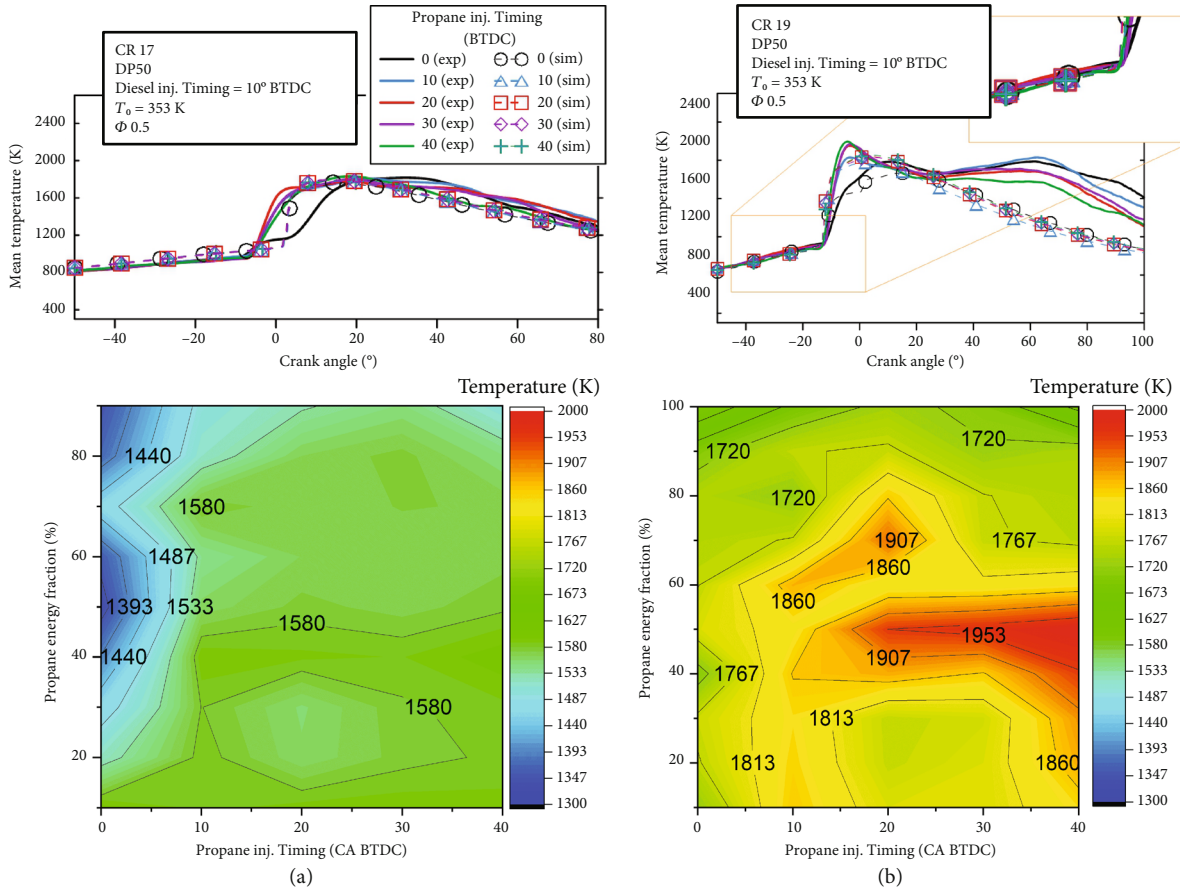

FIGURE 7: In-cylinder temperature under propane energy fraction 10-100%, propane injection timing 0°-40° BTDC and compression ratio of (a) 17 and (b) 19.

was produced in the main combustion area. This indicates the slow combustion of propane, even when it occurs after diesel autoignition process. The significant development of temperature mostly occurs after the diesel autoignition area. This can be observed by comparing the 0° BTDC propane injection timing with the other propane injection timing case. At 0° BTDC propane injection timing, a significant development of temperature occurred earlier compared to the other propane injection timing parameter. This indicates that the propane fuel does not provide autoignition behavior for the CR17 condition, which delayed the autoignition characteristics of the diesel. The propane was injected at ambient temperature 673 K at 40° BTDC, 721 K at 30° BTDC, 754 K at 20° BTDC, 773 K at 10° BTDC, and 1310 K at 0° BTDC. Even though propane injection exceeds the autoignition temperature of propane (481 K), a misfire was spotted for 100% energy fraction of propane. Better spray quality could improve autoignition characteristics of propane by increasing the injection pressure for future studies.

The development of temperature and max in-cylinder temperature of propane energy fraction and propane injection timing variation at CR19 is shown in Figure 8(b). Observing the development of in-cylinder temperature trace, we noticed that a significant development of temperature occurred earlier than diesel autoignition area for propane injection timing 40°-10° BTDC, which was much higher compared to CR17. This indicates the autoignition behavior of propane. Moreover, it occurs earlier than the autoignition of the diesel. The addition of propane produces higher temperature development in the early stage of combustion (before 0° CA). The second temperature increase was noticed at 28° CA for all propane injection timing cases. This seems that propane fuel did not undergo perfect combustion in the early stage of combustion. The low temperature of fuel reduces the ambient temperature. Moreover, propane injection in the liquid phase makes the heat transfer process harder. For that reason, LPG produces lower NO_x emission due to the lower temperature inside the engine [42], which agrees with previous studies using an LPG direct injection strategy [43]. An improvement of max in-cylinder temperature was noticed in CR19 for all SOI of propane and percentage propane energy fraction case. As mentioned before, the highest peak temperature was produced at CR19 in the early-stage reaction, which occurs in the BTDC area due to the reactivity of propane. In the mixing-controlled combustion area, there was not a significant difference in peak temperature. For that reason, there is an insignificant maximum temperature gradient in CR17 condition. Even so, there are similar behaviors of maximum in-cylinder temperature trace for both compression ratios. The steady improvement of maximum in-cylinder temperature was noticed under 50%

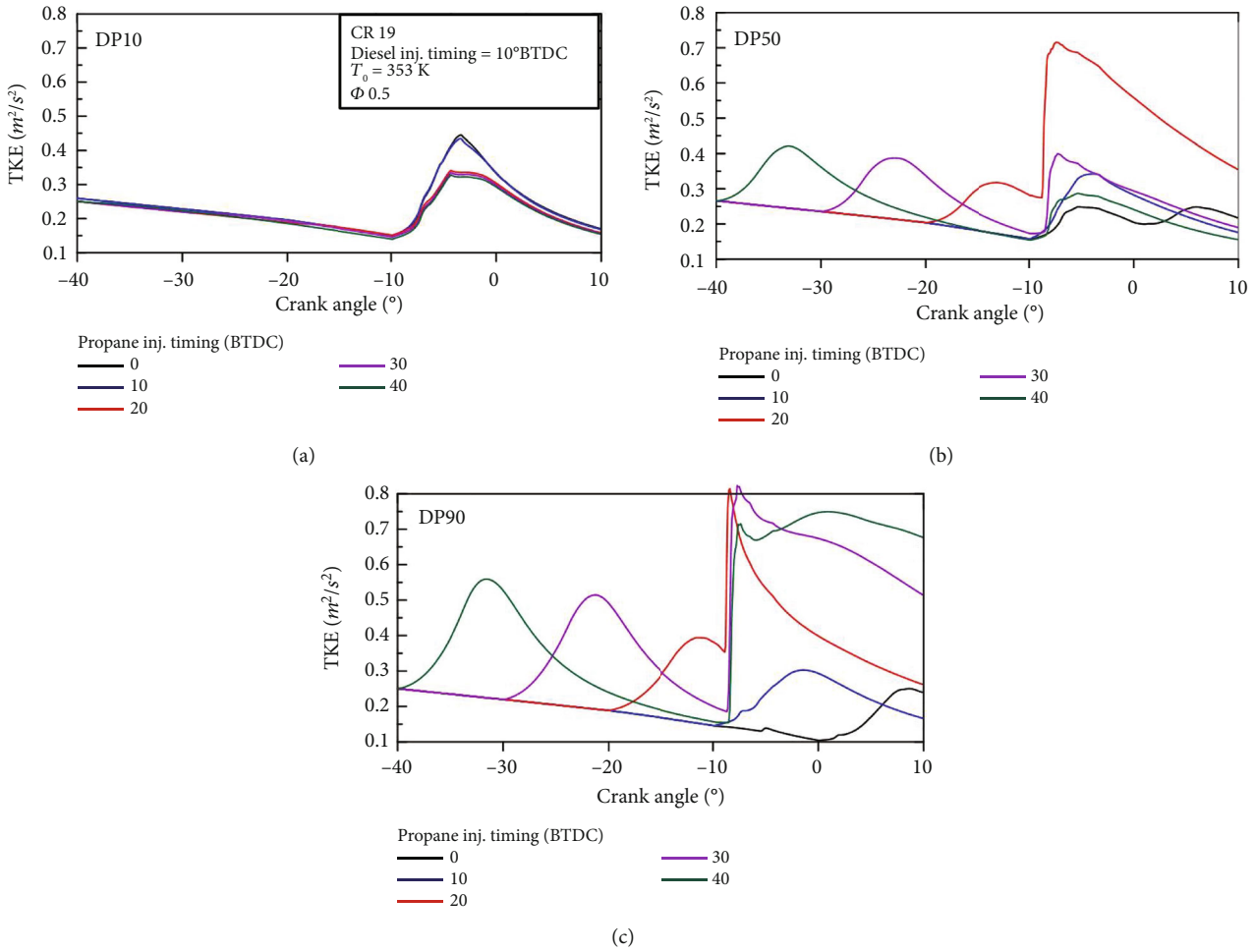

Figure 8: TKE flow pattern of dual direct injection fuel (diesel-propane) at CR19, propane energy fraction (a) 10%, (b) 50%, and (c) 90% and propane injection timing 0°-40°BTDC.

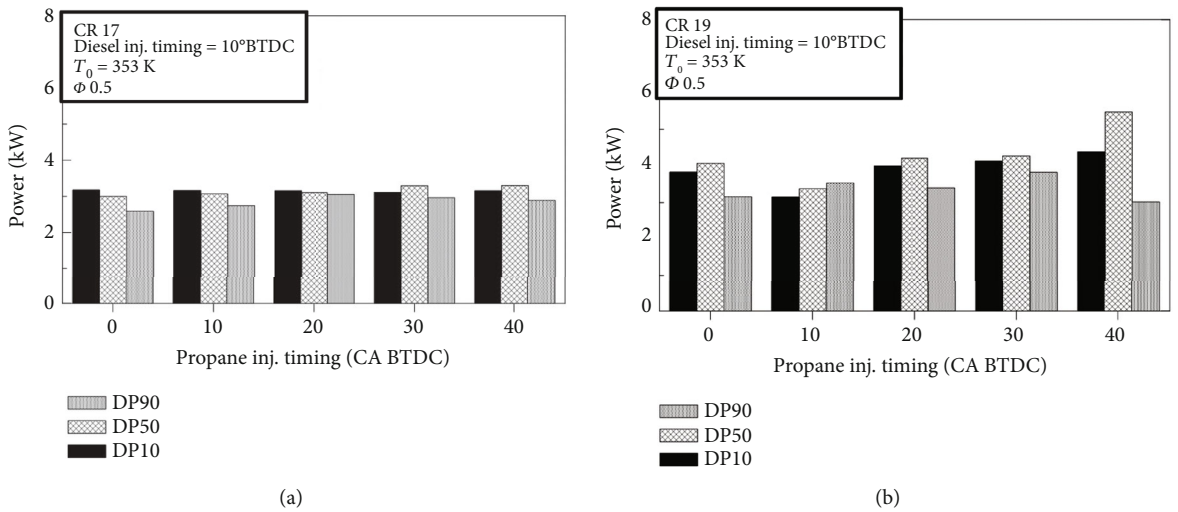

Figure 9: Power of RCEM for variations in (a) CR17 and (b) CR19, propane energy fraction and SOI of propane.

propane energy fraction by increasing the propane energy fraction and by injecting propane earlier than 20° BTDC. 10° BTDC propane injection timing produces slightly higher temperature compared to 0° BTDC and 20° BTDC propane injection timing. This is unaffected by ambient temperature degradation due to the early propane injection which improves

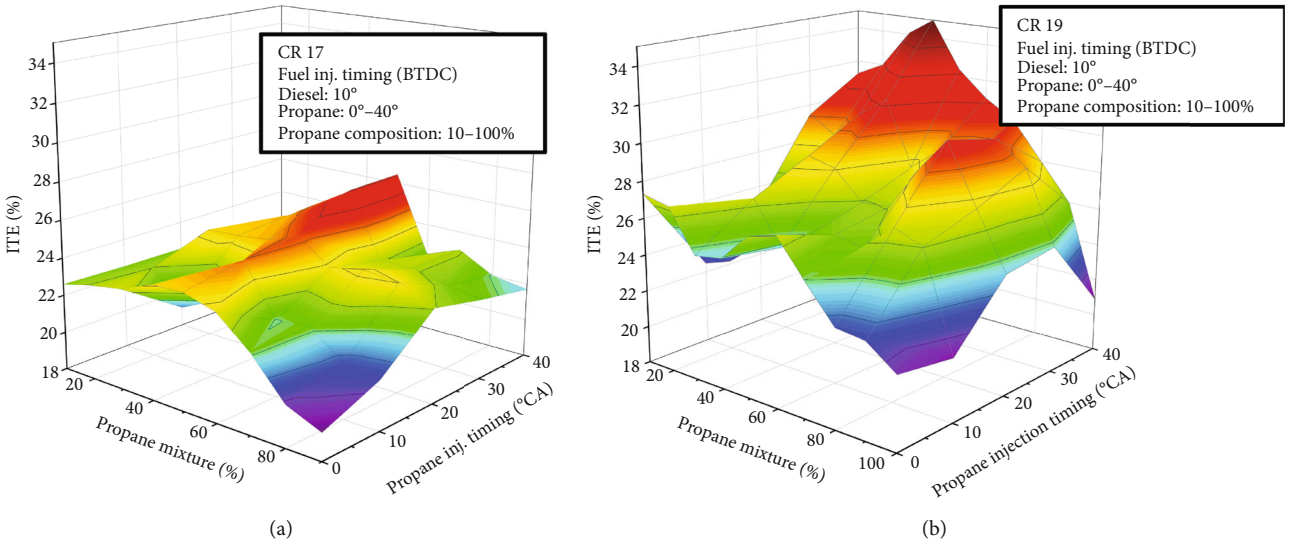

Figure 10: Thermal efficiency of RCEM under variation of (a) CR17 and (b) CR19, propane energy fraction and SOI of propane.

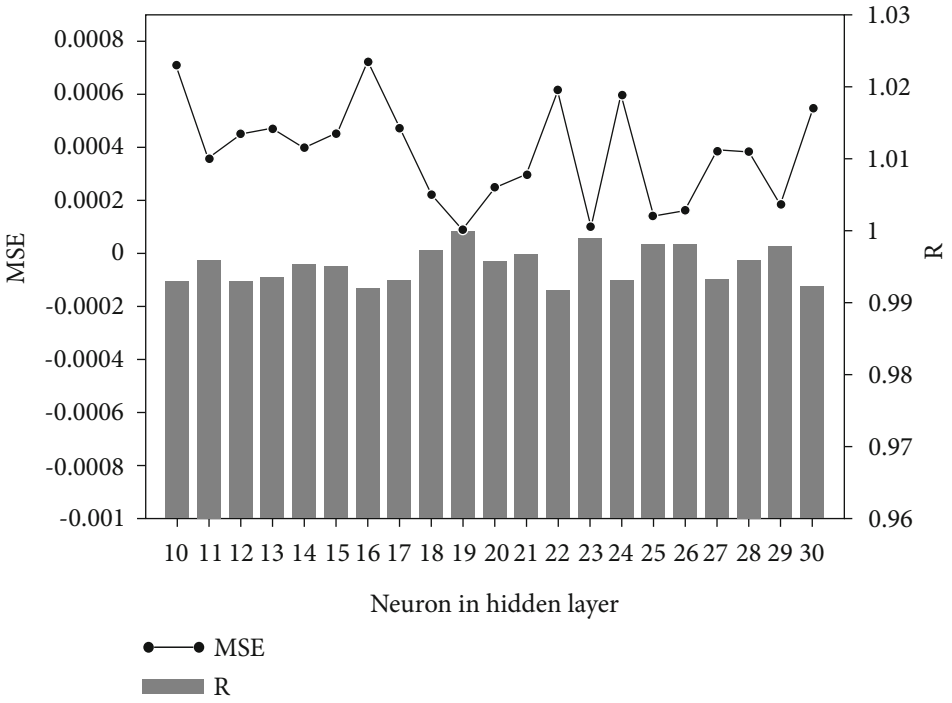

Figure 11: Validation MSE and R values for different neuron numbers in the hidden layer.

the autoignition characteristics of the diesel. The maximum in-cylinder temperature becomes lower as the propane energy fraction is greater than 50%. In this condition, earlier propane injection timing and lower maximum in-cylinder temperatures were produced.

Figure 8 shows the TKE at PD 10 (a), PD 50 (b), and PD 90 (c) with the variation of the SOI of propane. It shows the effect of propane fuel injection on the surrounding air flow and its effect before diesel injection, the moment of diesel injection, ignition, and a late propane injection event. The unaffected air flow from propane injection is also shown in the propane injection timing 10° and 0° BTDC. It can be used to compare standard TKE and TKE affected by propane injection. The TKE at 40° BTDC propane injection timing at 10° CA showed similar behavior compared to the TKE, which was unaffected by the propane injection. Degradation of TKE was observed after it reached the peak point, and it calmed down at the moment it reached the diesel injection timing. The 20° BTDC propane injection timing showed the highest TKE for all events. Diesel was injected when the TKE reached the highest point. A higher TKE contributes to a better air-fuel mixture and improved the autoignition characteristics of the fuels. This enhances the TKE at the main combustion event.

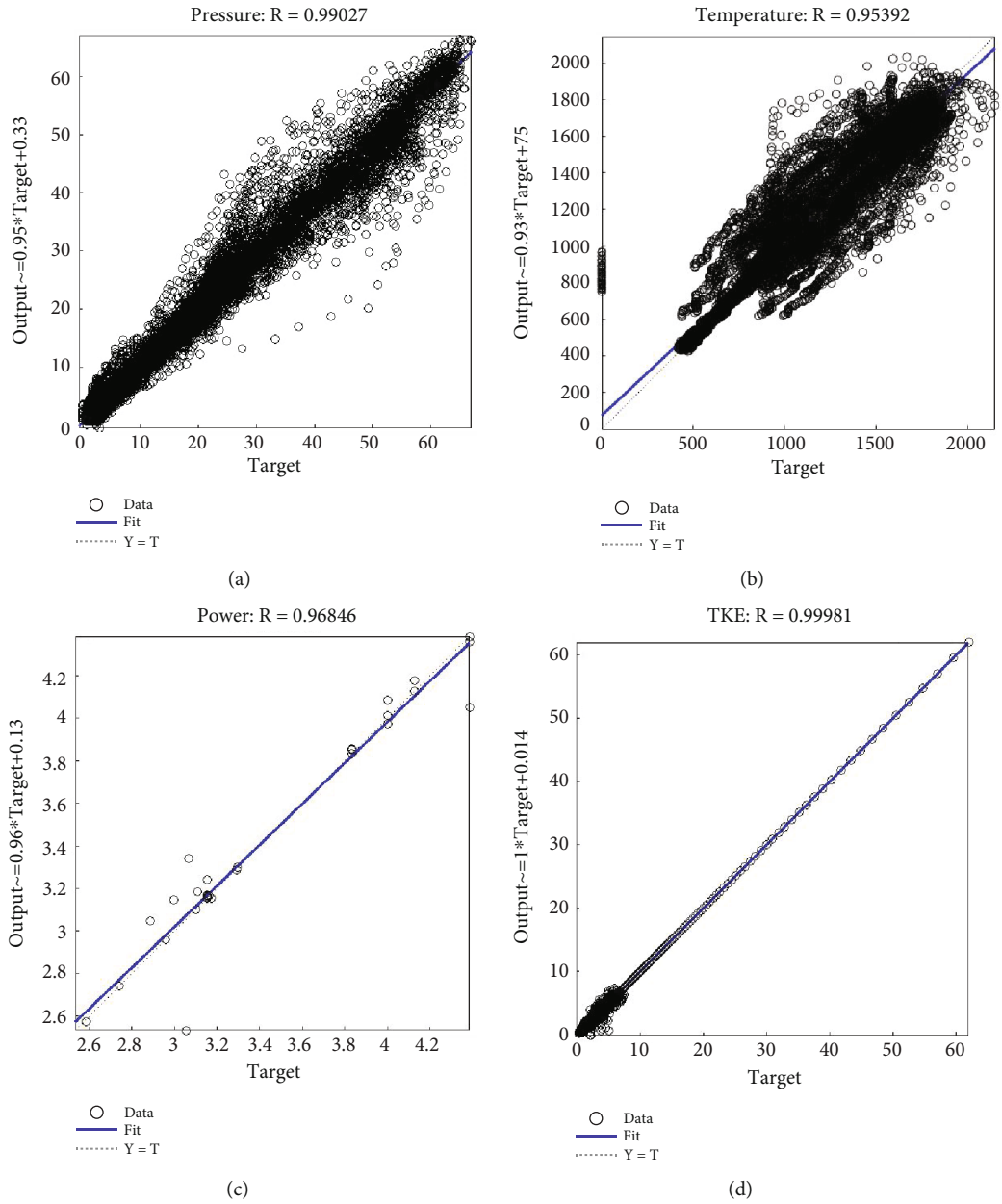

Figure 12: Continued.

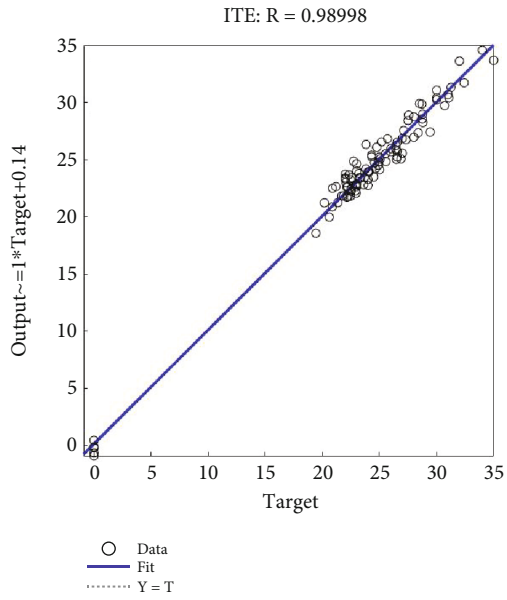

(e)

Figure 12: Plot of regression value of ANN performance for testing data prediction in 5 representative parameters: (a) pressure, (b) temperature, (c) power, (d) TKE, and (e) ITE.

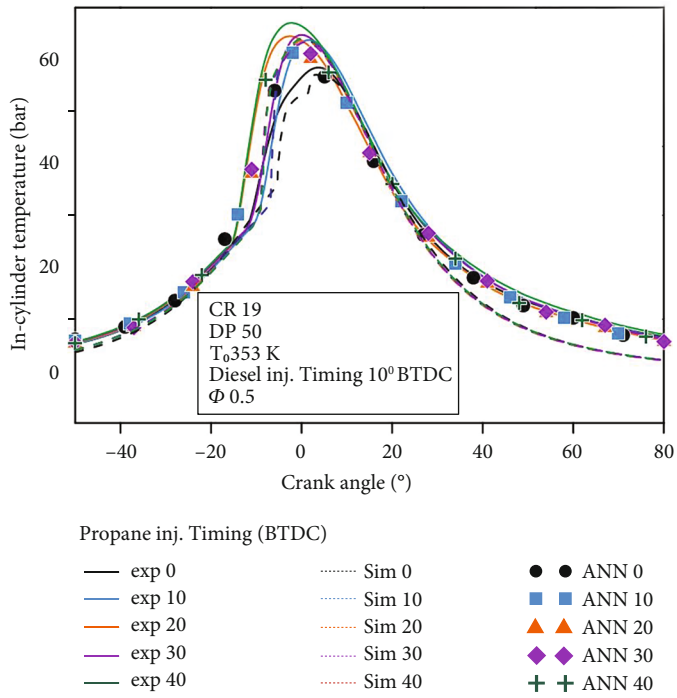

Figure 13: Plot of in-cylinder temperature of experiment, simulation, and ANN prediction.

Furthermore, we analyzed the power from the experiments using RCEM with dual direct injection applications shown at CR17 (Figure 9(a)) and CR19 (Figure 9(b)) with the variation of SOI of propane. A higher power output was obtained at a higher compression ratio. This also can be achieved by increasing the propane fraction up to 50% and by injecting propane earlier for both CR17 and CR19. A slight improvement in power was spotted at late propane injection timing in the lean fraction of propane, and it became stronger when a higher CR was applied. For rich fractions of propane, consistent degradation of power was observed for both CR17 and CR19. This behavior was also observed when early propane injection timing was applied.

Figure 10 shows the indicated thermal efficiency of the engine: Figure 10(a) compression ratio 17 and Figure 10(b) compression ratio 19 with the variation of injection timing from 0° to 40° BTDC and percentage of propane from 10 to 100%. The transition of compression ratio from 17 to 19

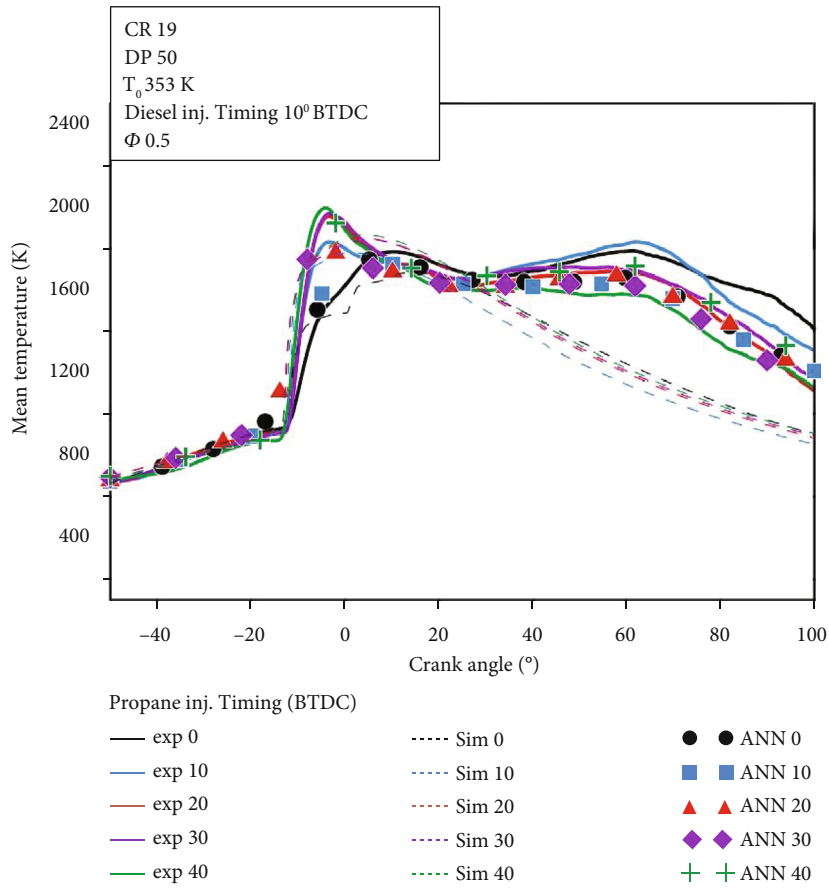

Figure 14: Plot of in-cylinder temperature of RCEM's experiment, simulation and ANN prediction data.

improved the ITE significantly. The ITE shows similar behavior for both compression ratios. The ITE for quantities of propane under 50% showed improvement when the propane was injected earlier. Applying a lower quantity of propane at a constant fuel injection pressure reduced the possibility of larger fuel spray droplets and an ambient temperature reduction. In this condition, earlier injection timing, which has longer ignition delay, produces a better air-fuel mixture and enhances the quality of combustion. In a lean mixture of propane, the lowest ITE was observed when the propane and diesel were injected at the same time (10° BTDC). An improvement in ITE was observed when propane was injected after diesel injection timing (0° BTDC).

For conditions with more than 50% propane, the early injection timing of propane produced a lower ITE. It requires higher ambient temperature and pressure as the proportion of propane increased due to the high-octane characteristics of propane. In nonreactive conditions, the liquid phase of the propane reduced the in-cylinder temperature and disturbed the diesel autoignition process. In early propane injection timing, the higher quantity of propane enhanced the possibility of in-cylinder wall wetting, causing a reduction in cylinder wall temperature, producing larger fuel droplets around the cylinder wall. This shows an improvement of ITE at propane injection timings of 20°-30° BTDC. There is significant degradation of ITE when propane was injected closer to TDC. The lowest ITE was produced when 100% propane was applied. The best ITE for CR17 and CR19 occurred at 40% propane and 40 propane injection timing.

3.2. Evaluation of ANN Results. The number of neurons in the hidden layer was changed to track changes in MSE without using a random ANN configuration (Figure 11). The MSE at 19 neurons in the hidden layer was lowest at 0.0000922 among neuron numbers of 10 to 30. As a result, the best model was an ANN with a 3-19-5 topological configuration that used the trainlm training algorithm and the feed-forward with backpropagation learning algorithm with a logsig transfer function. The learning rate is concerned with the intensity of reducing the error after iterations, which has an impact on the portion of the individual adjustment to the previous weight. A rapid learning process is achieved when the learning rate is set to a high number. The network may not learn well when there is a significant amount of input set instability. Setting the learning rate to a high value is actually improper and detrimental to learning [39].

The selected ANN model was trained to assess the accuracy of the cylinder pressure, rate of heat release, cumulative heat release, velocity of heat transfer, mass fraction burned, and average gas temperature combustion parameters. For training, testing, and validation purposes, the engine's experimental data for CCM and the DFC mode of 1-hexanol with diesel/biodiesel are divided into three sets of 70%, 15%, and

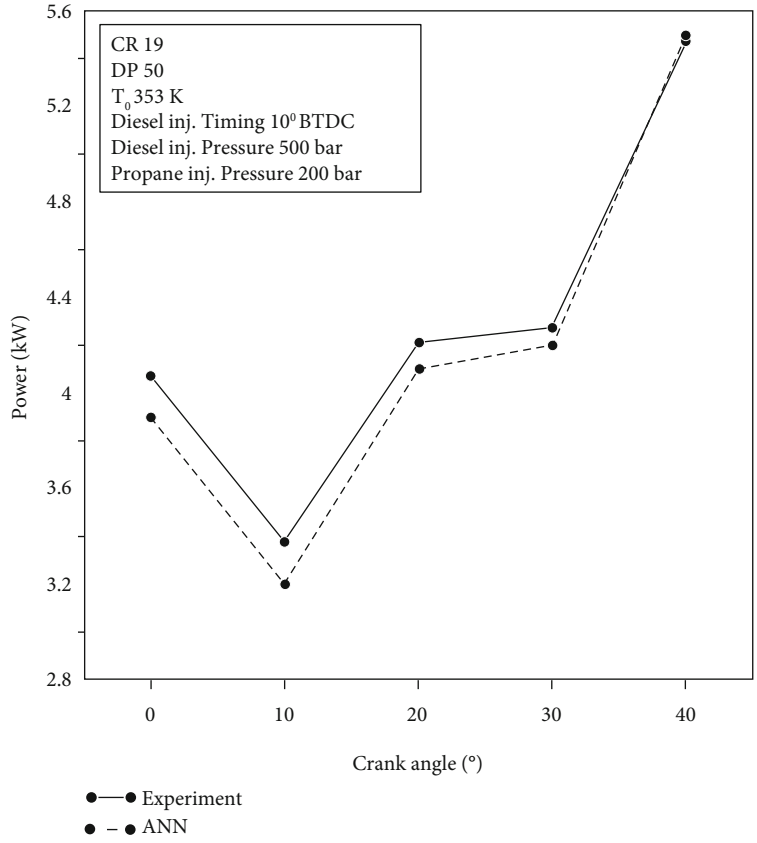

Figure 15: Plot of power of RCEM experiments, simulation, and ANN prediction data.

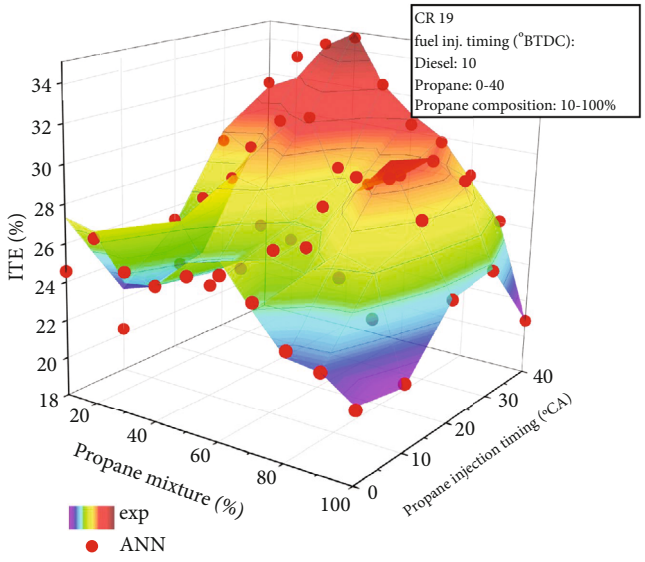

Figure 16: Plot of ITE of RCEM for experiment, simulation, and ANN prediction data.

15%, respectively [44]. Figure 12 makes it abundantly clear that the chosen ANN model was used to carry out reliable estimations for the previously mentioned combustion parameters. The highest R^2 of 0.99981 for TKE and the lowest R^2 of 0.96846 for power were obtained for training and testing conditions in the chosen ANN architecture, as shown in Figure 12: pressure (a), temperature (b), power (c), TKE (d), and ITE (e). The extremely close data points surrounding the unity line in Figure 12 show that the ANN was successful and robust. In the current study, we suggest a model based on the excellent ANN prediction of the obtained combustion values. The ANN model's predicted values were 0.00038 of MSE. The ANN model produced reliable predictions through 204 iterations.

3.3. Comparing Experimental Result and Discussion in ANN Modelling. Information from the experimental work is presented in this section, along with average gas temperature, mass fraction burned, rate of heat release, cumulative heat release, velocity of heat transfer, and cylinder pressure. The results for each parameter are displayed in two figures. The other compares experimental results with ANN values, while the first only contains experimental results. The experimental and ANN results are quite similar when all the figures were analyzed, and robust estimates were made to make predictions.

3.3.1. In-Cylinder Pressure. In-cylinder pressures of RCEMs employing dual direct injection fuel (diesel and propane) strategies at various propane SOIs are contrasted in Figure 13. The CFD modelling output of in-cylinder pressure reveals the underprediction in the expansion area. This demonstrates that CFD modelling cannot provide an exact prediction of the uncertainty of the unburned fuel during

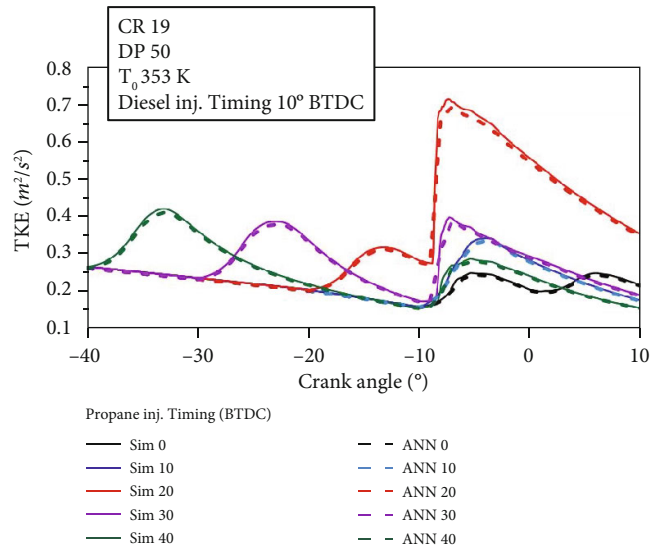

Figure 17: Plot of TKE of RCEM's experiment, simulations, and ANN prediction data.

ignition. The expansion phase's pressure and temperature were increased, and the combustion phase was prolonged. When compared to CFD modelling, the ANN modelling produced predictions that were more accurate. The prediction based on training and validating the data can increase the accuracy of the predicted data in addition to being produced faster and with fewer computer requirements. From 100 input data and 360000 total output sample data, the MSE was 0.942935.

3.3.2. In-Cylinder Temperature. Figure 14 depicts the mean temperature of RCEMs running on dual direct injection fuel (diesel and propane) strategies at various propane SOIs. The underprediction of data in the expansion state is more clearly observed in the mean temperature graph. When the fuel reaches the critical ignition point, the CFD modelling creates a chain reaction of combustion. The ignition process raises ambient temperature, which satisfies the requirement for fuel to reach temperatures higher than those required for autoignition. In the experimental process, some propane spray came out as an iced phase due to the significant temperature drop when the propane was maintained as the liquid phase. This causes different ignition temperatures in the iced spray region, which requires a higher ignition temperature. This phenomenon is ignored by CFD modelling, which results in underprediction in the expansion area. Hence, the developed ANN models have great potential to predict the real-time output values of the engine experiments. MSE was 0.837461 from 100 input data with 360000 total sample data.

Figure 15 shows the predicted values of power inside the RCEM at CR19, DP50, and SOI of propane 0-40° BTDC on an ANN model, based on 100 data input and 100 total sample data. The overall forecast trend is positive, and the ANN model is quite precise in forecasting output power with MSE 0.024579.

Figure 16 shows the thermal efficiency of the RCEM at CR19 and DP10-100 at SOI of propane 0°-40° BTDC. For 19 neurons in the hidden layer, the MSE was equal to 0.022405 for 100 data inputs and 100 total sample data. Power predictions showed similar accuracy. The R and MSE for experimental data reached the optimum accuracy when the set of output sample data was at the minimum number. The pressure and the temperature have 100 set sample data in which each sample consists of 3600 data as the trace of temperature and pressure data was recorded from -180° BTDC CA to 180° ATDC. The trace data causes uncertainty when the cycle of compression, combustion, and expansion occurs such as friction, graph distortion due to the electric disturbance, and the signal fluctuation of the sensor based on the electric current conversion. The data fluctuation from the pressure sensor is ±0.000002 bar during idle data acquisition. Even if the value of the discrepancy is small, the accumulation of the different fluctuations causes low accuracy prediction in terms of MSE and R values.

Figure 17 shows a comparison of the simulation and ANN prediction of TKE operated on RCEM on dual direct injection fuel strategy at CR19, PD50, and a SOI of propane at 0°-40° BTDC. The prediction of ANN shows a high accuracy compared to the TKE graph produced by the simulation; i.e., it showed an MSE of 0.003715 from 287900 sample data. Predictions on simulation data produced the highest accuracy compared to pressure and mean temperature prediction, which showed similarity in the number of output sample data. It even exceeds the prediction of power and ITE, which has the lowest output sample data. The minimum data set can improve the accuracy of the prediction since it can minimize the prediction from the uncertainty of experimental data. However, the data produced by the simulation produced the minimum uncertainty in the fluctuation pressure data due to the voltage conversion from the pressure sensor. The pressure data acquired from simulation has zero fluctuation when operated in idle conditions. This indicated that the accuracy of the prediction will improve as the number of output sample data increases. A comparison of the values of the MSE and R of TKE indicates its higher accuracy for ITE and power.

4. Conclusion

Propane 10%–100% by energy fraction under a dual direct injection fuel strategy was examined using experimentally measured data of an engine combustion process for various engine operating conditions. The propane SOI ranged from 0 to 40 BTDC, and the compression ratio was between 17 and 19. To forecast the combustion process parameters, an engine combustion model was created using CONVERGE software's ANN and CFD. Experimental and predicted results were compared to determine the prediction accuracy. The best ANN structure was established prior to training and validating the ANN with data from engine trials. We reached the following conclusions:

(1) Five parameters—pressure, temperature, power, TKE, and ITE—that were extracted from the engine performance map could be predicted by ANN with R values of 0.99027, 0.95392, 0.96846, 0.99981, and 0.98998 and MSE values of 0.942935, 0.837461, 0.024579, 0.022405, and 0.003715, respectively, which shows accurate forecasting of output data

(2) The simulation data shows the underprediction on the expansion process when compared to the experimental data. Meanwhile, the ANN prediction shows a better level of accuracy for the whole cycle trace

(3) The prediction data based on the in-cylinder trace experimental phenomena such as in-cylinder pressure and mean temperature produced a lower MSE compared to the data based on calculations such as power and ITE. The data acquired from the sensor showed fluctuations in the data due to the electric conversion which increases the errors of the prediction

(4) According to the prediction of the TKE, the ANN prediction of the in-cylinder trace phenomenon using the simulation output data samples had the highest accuracy

(5) ANN generalization capability is relatively high even when operating in previously unexplored areas of engine performance if trained with sufficiently large databases. The dependability of the developed ANN methodology was demonstrated even when tested under real-world, dynamic performance conditions

Nomenclature

RCEM: Rapid compression-expansion machine
BTDC: Before top dead center
CI: Compression ignition
DP: Diesel-propane
SI: Spark ignition
EoC: End of combustion
LHV: Low heating value
CN: Cetane number
TDC: Top dead center
BDC: Bottom dead center
ANN: Artificial neural network
MSE: Mean square error
SOI: Start of injection
SoC: Start of combustion
TKE: Turbulence kinetic energy
CR: Compression ratio
ϕ: Equivalence ratio
ITE: Indicated thermal efficiency
rpm: Rotations per minute.

Data Availability

The experimental data used to support the findings of this study are available from the corresponding author upon request.

Conflicts of Interest

The authors declare that they have no conflicts of interest.

Acknowledgments

This work was supported by the "Regional Innovation Strategy (RIS)" through the National Research Foundation of Korea (NRF) funded by the Ministry of Education (MOE) (2021RIS-003). This work was supported by the National Research Foundation (NRF) of Korea grant funded by the Korea government (MSIT) (No. RS-2023-00281590).

References

[1] D. B. Lata, A. Misra, and S. Medhekar, "Investigations on the combustion parameters of a dual fuel diesel engine with hydrogen and LPG as secondary fuels," *International Journal of Hydrogen Energy*, vol. 36, no. 21, pp. 13808–13819, 2011.

[2] S. V. Channapattana, S. Campli, A. Madhusudhan, S. Notla, R. Arkerimath, and M. K. Tripathi, "Energy analysis of DI-CI engine with nickel oxide nanoparticle added azadirachta indica biofuel at different static injection timing based on exergy," *Energy*, vol. 267, article 126622, 2023.

[3] G. J. Suppes and T. S. Storvick, "Chapter 5- The new electric vehicle society," in *Sustainable Power Technologies and Infrastructure*, pp. 161–190, Academic Press, Boston, 2016.

[4] J. Jeon and S. Park, "Effects of pilot injection strategies on the flame temperature and soot distributions in an optical CI engine fueled with biodiesel and conventional diesel," *Applied Energy*, vol. 160, pp. 581–591, 2015.

[5] C. Lim, D. Kim, C. Song, J. Kim, J. Han, and J.-S. Cha, "Performance and emission characteristics of a vehicle fueled with enriched biogas and natural gases," *Applied Energy*, vol. 139, pp. 17–29, 2015.

[6] M. Huth and A. Heilos, "14- Fuel flexibility in gas turbine systems: impact on burner design and performance," in *Modern Gas Turbine Systems*, P. Jansohn, Ed., pp. 635–684, Woodhead Publishing, 2013.

[7] S. Murillo, J. L. Miguez, J. Porteiro, L. M. L. González, E. Granada, and J. C. Morán, "LPG: pollutant emission and performance enhancement for spark-ignition four strokes outboard engines," *Applied Thermal Engineering*, vol. 25, no. 13, pp. 1882–1893, 2005.

[8] P. Nieuwenhuis and P. Wells, "6-Powertrain and fuel," in *The Automotive Industry and the Environment*, P. Nieuwenhuis and P. Wells, Eds., pp. 73–86, Woodhead Publishing, 2003.

[9] H. Ambarita, "Performance and emission characteristics of a small diesel engine run in dual-fuel (diesel-biogas) mode," *Case Studies in Thermal Engineering*, vol. 10, pp. 179–191, 2017.

[10] S. Ouchikh, M. S. Lounici, L. Tarabet, K. Loubar, and M. Tazerout, "Effect of natural gas enrichment with hydrogen on combustion characteristics of a dual fuel diesel engine," *International Journal of Hydrogen Energy*, vol. 44, no. 26, pp. 13974–13987, 2019.

[11] A. Igbojionu, C. Anyadiegwu, E. Anyanwu, B. Obah, and C. Muonagor, "Technical and economic evaluation of the use of CNG as potential public transport fuel in Nigeria," *Scientific African*, vol. 6, article e00212, 2019.

[12] F. Z. Aklouche, K. Loubar, A. Bentebbiche, S. Awad, and M. Tazerout, "Predictive model of the diesel engine operating in dual-fuel mode fuelled with different gaseous fuels," *Fuel*, vol. 220, pp. 599–606, 2018.

[13] S. S. Goldsborough, S. Hochgreb, G. Vanhove, M. S. Wooldridge, H. J. Curran, and C.-J. Sung, "Advances in rapid compression machine studies of low- and intermediate-temperature autoignition phenomena," *Progress in Energy and Combustion Science*, vol. 63, pp. 1–78, 2017.

[14] D. Jian, G. Xiaohong, L. Gesheng, and Z. Xintang, *Study on Diesel-LPG Dual Fuel Engines*, SAE Technical Paper, 2001.

[15] N. K. M. Jothi, G. Nagarajan, and S. Renganarayanan, "Experimental studies on homogeneous charge CI engine fueled with LPG using DEE as an ignition enhancer," *Renewable Energy*, vol. 32, no. 9, pp. 1581–1593, 2007.

[16] S. Goto, D. Lee, Y. Wakao et al., "Development of an LPG DI diesel engine using cetane number enhancing additives," *SAE Transactions*, vol. 108, pp. 1941–1950, 1999.

[17] K. Hashimoto, H. Ohta, T. Hirasawa, M. Arai, and M. Tamura, "Evaluation of ignition quality of LPG with cetane number improver," *SAE Transactions*, vol. 111, pp. 1462–1466, 2002.

[18] T. Vinoth, P. Vasanthakumar, J. Krishnaraj, S. K. Arunsankar, J. Hariharan, and M. Palanisamy, "Experimental investigation on LPG+ diesel fuelled engine with DEE ignition improver," *Materials Today: Proceedings*, vol. 4, no. 8, pp. 9126–9132, 2017.

[19] M. M. Musthafa, "A comparative study on coated and uncoated diesel engine performance and emissions running on dual fuel (LPG–biodiesel) with and without additive," *Industrial Crops and Products*, vol. 128, pp. 194–198, 2019.

[20] F. Oliva and D. Fernández-Rodríguez, "Autoignition study of LPG blends with diesel and HVO in a constant-volume combustion chamber," *Fuel*, vol. 267, article 117173, 2020.

[21] R. K. Mehra, H. Duan, S. Luo, A. Rao, and F. Ma, "Experimental and artificial neural network (ANN) study of hydrogen enriched compressed natural gas (HCNG) engine under various ignition timings and excess air ratios," *Applied Energy*, vol. 228, pp. 736–754, 2018.

[22] C. Grosan, A. Abraham, C. Grosan, and A. Abraham, "Artificial neural networks," *Intelligent Systems: A Modern Approach*, pp. 281–323, 2011.

[23] C. Srinidhi, A. Madhusudhan, S. V. Channapattana, S. V. Gawali, and K. Aithal, "RSM based parameter optimization of CI engine fuelled with nickel oxide dosed Azadirachta indica methyl ester," *Energy*, vol. 234, article 121282, 2021.

[24] C. Srinidhi, S. Panshetty, Madhusudhan, and S. V. Channapattana, "Optimization of neem biodiesel blend and injection pressure of CI engine," in *Advances in Structures, Systems and Materials*, Lecture Notes on Multidisciplinary Industrial Engineering, M. Vinyas, A. Loja, and K. Reddy, Eds., Springer, Singapore, 2020.

[25] T. Y. G. Vidal, N. A. Claude Valery, A. N. Emmanuel et al., "Performance map of a LPG-diesel dual-fuel engine based on experimental and non-linear least squares determined wiebe function," *Scientific African*, vol. 13, article e00900, 2021.

[26] A. Boretti, "Numerical study of the substitutional diesel fuel energy in a dual fuel diesel-LPG engine with two direct injectors per cylinder," *Fuel Processing Technology*, vol. 161, pp. 41–51, 2017.

[27] C.-J. Sung and H. J. Curran, "Using rapid compression machines for chemical kinetics studies," *Progress in Energy and Combustion Science*, vol. 44, pp. 1–18, 2014.

[28] S. Jeong, W. Kim, C. Oh et al., "An experimental study on the clutch-type water pump of diesel passenger vehicle for reducing fuel consumption and CO_2 emission," in *Proceedings of the ASME-JSME-KSME 2011 Joint Fluids Engineering Conference. ASME-JSME-KSME 2011 Joint Fluids Engineering Conference: Volume 1, Symposia – Parts A, B, C, and D*, pp. 893–903, Hamamatsu, Japan, 2011.

[29] D. H. Qi, B. Chen, and D. Zhang, "Combustion and exhaust emissions characteristics of a dual-fuel compression ignition engine operated with diesel fuel and liquefied petroleum gas," *Journal of Energy Engineering*, vol. 142, no. 4, article 4016017, 2016.

[30] Z. Han and R. D. Reitz, "Turbulence modeling of internal combustion engines using RNG κ-ε models," *Combustion Science and Technology*, vol. 106, no. 4–6, pp. 267–295, 1995.

[31] B. S. de Lima, K. C. Fagundes, G. R. C. Faria, M. H. B. Sandoval, and C. E. C. Alvarez, *ENCIT2018-0458 analysis of the combustion process in an engine adapted with prechamber using a zero dimensional numerical model and a three-dimensional model*17th Brazilian Congress of Thermal Sciences and Engineering.

[32] R. D. Reitz, "Mechanism of breakup of round liquid jets," *Encyclopedia of Fluid Mechanics*, vol. 10, 1986.

[33] D. P. Schmidt and C. J. Rutland, "A new droplet collision algorithm," *Journal of Computational Physics*, vol. 164, no. 1, pp. 62–80, 2000.

[34] A. A. Amsden, P. J. O'Rourke, and T. D. Butler, *KIVA-II: A computer program for chemically reactive flows with sprays*, Los Alamos National Lab.(LANL), Los Alamos, NM (United States), 1989.

[35] C. Windarto and O. Lim, "Spark discharge energy effect on in-cylinder characteristics performance of rapid compression and expansion machine with spark ignition direct injection strategy," *Fuel*, vol. 337, article 127165, 2023.

[36] H. K. Aasi and M. Mishra, "Experimental investigation and ANN modelling on thermo-hydraulic efficacy of cross-flow three-fluid plate-fin heat exchanger," *International Journal of Thermal Sciences*, vol. 164, article 106870, 2021.

[37] M. Aydın, S. Uslu, and M. B. Çelik, "Performance and emission prediction of a compression ignition engine fueled with biodiesel-diesel blends: a combined application of ANN and RSM based optimization," *Fuel*, vol. 269, article 117472, 2020.

[38] S. Bhowmik, R. Panua, D. Debroy, and A. Paul, "Artificial neural network prediction of diesel engine performance and

emission fueled with diesel–kerosene–ethanol blends: a fuzzy-based optimization," *Journal of Energy Resources Technology*, vol. 139, no. 4, article 42201, 2017.

[39] H. Taghavifar, H. Taghavifar, A. Mardani, A. Mohebbi, and S. Khalilarya, "A numerical investigation on the wall heat flux in a DI diesel engine fueled with n-heptane using a coupled CFD and ANN approach," *Fuel*, vol. 140, pp. 227–236, 2015.

[40] K. S. Varde, *Ignition Delay and Emissions Characteristics of a Methanol-Diesel Fueled Engine at Low Charge Temperatures*, SAE Technical Paper, 1992.

[41] S. H. Park, H. J. Kim, and C. S. Lee, "Comparison of experimental and predicted atomization characteristics of high-pressure diesel spray under various fuel and ambient temperature," *Journal of Mechanical Science and Technology*, vol. 24, no. 7, pp. 1491–1499, 2010.

[42] M. R. Aosaf, Y. Wang, and K. Du, "Comparison of the emission factors of air pollutants from gasoline, CNG, LPG and diesel fueled vehicles at idle speed," *Environmental Pollution*, vol. 305, article 119296, 2022.

[43] S. Baek, K. Kim, J. Cho, C.-L. Myung, and S. Park, "Assessment of gaseous, particulate, and unregulated emissions from diesel compression ignition and LPG direct injection spark ignition minibus vehicles under the world harmonized vehicle cycle on a chassis dynamometer," *Fuel*, vol. 294, article 120392, 2021.

[44] D. Babu, V. Thangarasu, and A. Ramanathan, "Artificial neural network approach on forecasting diesel engine characteristics fuelled with waste frying oil biodiesel," *Applied Energy*, vol. 263, article 114612, 2020.